IMECE2011-62151

SIZE EFFECTS DURING FEMTOSECOND LASER INTERACTION WITH NANOSIZED METAL PARTICLES

Jing Huang, Yuwen Zhang[1,2,3]**, and J.K. Chen**[2,3]
Department of Mechanical and Aerospace Engineering
University of Missouri
Columbia MO 65211, USA

ABSTRACT

To obtain more in-depth knowledge about the microscopic process during laser sintering, phase change processes including melting, evaporation and resolidification during the irradiation of femtosecond laser on nanosized gold particles were simulated. Laser heat source term was revised to be in accordance with the spherical coordinates and actual situation in a sintering powder bed. The effects of multiple reflection and pulse energy overlapping in small particle size were considered. The results show that, when the particle size is big enough, the simulation results match those of old model. When the particle size is small and laser fluence is high, no resolidification takes place in the time range of the simulation. The laser fluence range to achieve partial melting is narrow when the particle is small. When the diameter is smaller than 400 nm, temperature gradient during the heating period is ignorable, which is different from the large particles. The threshold value of laser fluence to achieve vaporization is about two times higher than that of melting with the same particle size.

INTRODUCTION

Selective Laser Sintering (SLS) utilizes the advantage of high energy density, precise control characteristics of laser beams to fuse powdered material layer by layer to build a desired part. SLS is ideal for fast fabrication of prototype parts to shorten the development period for new products. It can also fabricate complex structures that traditional methods cannot build. Another advantage of SLS lies in its ability to process a wide range of powder materials, including polymers, metals and composites. For metallic powders which the current work is concerned, particles are joined via melting and resolidification.

SLS has developed very rapidly since it was invented in the late 1980s [1-3] and many commercial systems are available in market now. A review of most recent SLS advances was presented by Kumar [4]. However, there are still some problems with SLS to limit it from mass production of end-use parts. Balling phenomenon is one, which impairs high quality surface finish and good mechanical properties [5]. Balling phenomenon takes place when melted powder grains stick to each other because of surface tension forces and forms metal spheres along the scanning path. There are two methods to deal with this problem. The first is to use two different kinds of powders that have different melting points. Appropriate laser irradiation can melt the low-melting point powder and bond high-melting point particles together [6, 7]. Another approach is to use a pulsed laser instead of a continuous wave [8-10] to melt on the skin of the single-melting powder to join them together. Pulsed laser can lead to better precision, which can be explained by shorter liquid phase existence and evaporation recoil force that can overcome the surface tension force [10].

Numerous experimental studies have been performed to enhance the quality of SLS, with a wide range of laser types, powder material, sizes and scanning strategies [8, 9, 11]. Fischer et al. carried out a series of experimental study on sintering of Titanium powders with pulsed Nd-YAG laser [12-16]. The application of SLS on manufacturing biocompatible implant parts also attracted some attentions [17].

Many theoretical models were put forward to simulate the sintering process. They can be divided into two categories. The first category treats the powder bed as continuum media and studies the macroscopic behavior of the sintering process, such

as heat affected zone, melting pool size, surface motion, etc. Gusarov studied the radiation transfer in the powder bed by treating powder bed as a continuum medium [18]. Yilbas presented a 3-dimensional model to simulate the phase change in a powder bed [19, 20]. Rostaml and Raisi obtained the temperature distribution and melting pool size numerically and compared them with experiment results [21]. The second category deals with the irradiation on single or multiple particles. Fischer et al. studied the heat transfer process in a single particle through a simple model [22]. However the particle size is relatively large, around 102 μm in diameter and phase change of the particle was not considered. Petrushina built up a multiple particle model to study the sintering process, but only temperature distribution was simulated, phase change was not considered [23]. Zhang and co-workers studied the phase change phenomena when a single metal particle was irradiated by nano to pico-second pulsed laser. The influences of laser duration, fluence and particle size on the melting, vaporization and resolidification process were investigated [24-26] .

In this paper, the irradiation of femtosecond pulsed laser on a single nanosized particle is simulated numerically. For the rapid melting and resolidification processes, nucleation dynamics is employed to delineate the proceeding of solid-liquid interface. For the evaporation process, a thermodynamic model based on wave hypothesis is utilized. The simulation focuses on the size effect of nano-sized particles. Different particle size and laser fluence are used to study their effects on the phase change processes including melting, vaporization and resolidification.

NOMENCLATURE

Be	coefficient for electron heat capacity (J/m^3-K^2)
C	heat capacity (J/m^3-K)
c_p	specific heat (J/kg-K)
G	electron-lattice coupling coefficient (W/m^3-K)
h	latent heat of phase change (J/kg)
J	laser fluence (J/m^2)
J_0	directional laser fluence (J/m^2)
k	thermal conductivity (W/m-K)
L	thickness of the metal film (m)
M	molar mass (kg/kmol)
p	pressure (Pa)
q''	heat flux (W/m^2)
r	radial coordinate (m)
R	reflectivity
r_0	radius of particle (m)
R_g	specific gas constant (J/kg-K)
R_u	universal gas constant (J/kmol-K)
s	interfacial location (m)
S	intensity of the internal heat source (W/m^3)
t	time (s)
t_p	pulse width (s)
T	temperature (K)
T_F	Fermi temperature (K)
u	interfacial velocity (m/s)
V_0	interfacial velocity factor (m/s)

Greek Symbols

δ	optical penetration depth (m)
δ_b	ballistic range (m)
ε	total emissivity
ρ	density (kg/m^3)
σ	Stefan-Boltzmann constant (W/m^2 -K^4)

Superscripts

0	last time step

Subscripts

e	electron
eq	thermal equilibrium state
i	initial condition
l	lattice
ℓ	liquid
ℓv	liquid-vapor interface
m	melting
R	thermal radiation
s	solid
$s\ell$	solid-liquid interface
sur	surface
∞	ambient environment

PHYSICAL MODEL

Figure 1 shows the physical model under consideration. A laser pulse is deposited on a powder bed with initial temperature of T_i. Because of scattering, reflection and
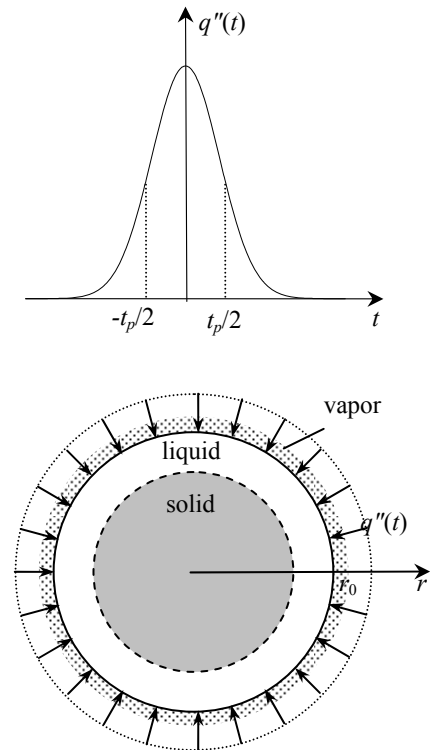

Fig. 1 Physical model for ultrafast phase change

penetration of the laser beams, it is assumed that at any vacant space in the powder bed, laser radiation distribute in all direction evenly. [25, 26] For any point on a single particle surface, it receives laser radiation from all different directions with the same energy density. Therefore, the problem can be approximated to 1-dimensional in the radial direction.
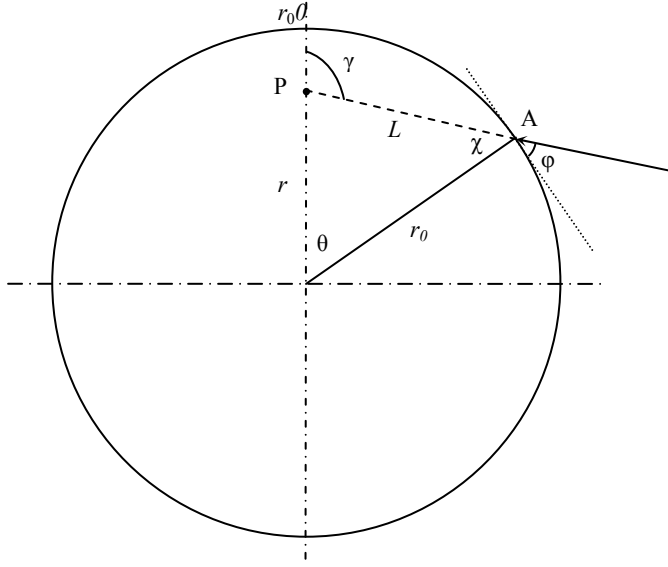

Fig. 2 Laser interaction with nanosized metal particle

Following the two-temperature model, the temperatures of electrons and lattice are calculated separately and coupled by a term proportional to temperature difference between electrons and lattice. [27, 28] Since only laser pulses with duration 100 fs are considered, the heat conductions in both electron and lattice are assumed to be parabolic. [24]

The energy equations of the free electrons and lattice are

$$C_e \frac{\partial T_e}{\partial t} = \frac{1}{r^2} \frac{\partial}{\partial r} \left(r^2 k_e \frac{\partial T_e}{\partial r} \right) - G(T_e - T_l) + S_0 \tag{1}$$

$$C_l \frac{\partial T_l}{\partial t} = \frac{1}{r^2} \frac{\partial}{\partial r} \left(r^2 k_l \frac{\partial T_l}{dr} \right) + G(T_e - T_l) \tag{2}$$

The heat capacity of electron C_e, as suggest by Chen et al. [29], is approximated by

$$C_e = \begin{cases} B_e T_e, & T_e < T_F/\pi^2 \\ 2B_e T_e/3 + C_e'/3, & T_F/\pi^2 \le T_e < 3T_F/\pi^2 \\ Nk_B + C_e'/3, & 3T_F/\pi^2 \le T_e < T_F \\ 3Nk_B/2, & T_e \ge T_F \end{cases} \tag{3}$$

where

$$C_e' = B_e T_F/\pi^2 + \frac{3Nk_B/2 - B_e T_F/\pi^2}{T_F - T_F/\pi^2} \left(T_e - T_F/\pi^2 \right) \tag{4}$$

The thermal conductivity of electron k_e can be obtained by [30]:

$$k_e = \chi \frac{\left(\vartheta_e^2 + 0.16 \right)^{5/4} \left(\vartheta_e^2 + 0.44 \right) \vartheta_e}{\left(\vartheta_e^2 + 0.092 \right)^{1/2} \left(\vartheta_e^2 + \eta \vartheta_l \right)} \tag{5}$$

where $\vartheta_e = T_e/T_F$ and $\vartheta_l = T_l/T_F$. Equation (5) is valid even if the electron temperature is comparable to the Fermi temperature, which is 6.42×10^4 K for gold. For the cases that $\vartheta_e \ll 1$, eq. (5) reduces to

$$k_e = k_{eq} \left(\frac{T_e}{T_l} \right) \tag{6}$$

For the metal at thermal equilibrium state, its thermal conductivity, k_{eq}, is the sum of the electron thermal conductivity, k_e, and the lattice thermal conductivity, k_l. In most cases k_e dominates k_{eq} because free electrons contribute to the majority part of heat conduction, For gold, k_l is usually taken to be 1% of k_{eq} [31], i.e.,

$$k_l = 0.01 k_{eq} \tag{7}$$

In eqs. (1) and (2), G is the electron-lattice coupling factor, which accounts for the heat transfer from hot electrons to lattice through collisions. Instead of a constant value, a phenomenological temperature-dependent G suggested by Chen et al. [32] is adopted:

$$G = G_{RT} \left[\frac{A_e}{B_l} \left(T_e + T_l \right) + 1 \right] \tag{8}$$

Since the electrons are more likely to collide with liquid atoms than the atoms in solid crystals, in the liquid phase, G, is taken to be 20% higher than that of the solid [33].

The laser irradiation is considered as a source term S_0 in eq. (1). As shown in Fig. 2, for any point P inside the particle, it receives irradiation from all direction. With the origin point placed at the center of the spherical particle, 1-Dimensional spherical coordinates is employed. It is assumed that: (1) the attenuation of laser energy in metal follows Beer-Lambert law, (2) The refraction angle is neglected, and (3) The laser pulse is of Gaussian in time domain and the full width at half maximum (FWHM) and directional fluence of the laser beam are t_p and J_0, respectively. The heat source per volume caused by laser irradiation on any point r is an integration on all directions:

$$S_0 = \int_0^{2\pi} \int_0^{2\pi} \left\{ 0.94 J_0 \frac{1-R}{t_P(\delta + \delta_b)} \exp \left[-\frac{L}{(\delta + \delta_b)} - 2.77 \left(\frac{t}{t_p} \right)^2 \right] \right\} \sin\varphi \, d\gamma \, d\omega \tag{9}$$

where ω is the azimuth angle, R is the reflectivity of the thin film, δ is the optical penetration depth, J is the laser pulse fluence, and δ_b is the ballistic depth. Wellershoff et al. [34] demonstrated that inclusion of ballistic motion of hot electrons led to a better simulation results to fit the experimental data, because the ballistic motion and brings incident energy into a much deeper part of the film. L and φ can be expressed as function of r and γ by the following equations:

$$L = \sqrt{X^2 + (Y-r)^2}$$

$$\sin\varphi = \frac{Y}{r_0}\cos\gamma + \frac{X}{r_0}\sin\gamma$$

$$X = -r\cot\gamma\sin^2\gamma + \sin^2\gamma\sqrt{-r^2 + r_0^2 + r_0^2\cot^2\gamma}$$

$$Y = r - r\cot^2\gamma\sin^2\gamma + \sin^2\gamma\cot\gamma\sqrt{-r^2 + r_0^2 + r_0^2\cot^2\gamma} \tag{10}$$

All the calculations start from $-2t_p$. A uniform temperature distribution is set to be the initial condition:

$$T_e(r, -2t_p) = T_l(r, -2t_p) = T_i \tag{11}$$

Axisymmetric condition is applied to the center ($r = 0$). On the surface of the particle ($r = r_0$) which receives laser irradiation, the heat loss caused by radiation will be considered.

$$\left.\frac{\partial T_e}{\partial r}\right|_{r=0} = \left.\frac{\partial T_l}{\partial r}\right|_{r=0} = 0 \tag{12}$$

$$q_R''\big|_{r=r_0} = \sigma\varepsilon(T_{sur}^4 - T_\infty^4) \tag{13}$$

Before evaporation takes place, T_{sur} is the surface lattice temperature at $r = r_0$. After evaporation begins, T_{sur} is the liquid-vapor interface temperature.

For rapid melting/solidification processes, the solid-liquid interfacial velocity is dominated by nucleation dynamics, instead by energy balance [35]. For short-pulsed laser melting of gold, the velocity of the solid-liquid interface is described by [33]

$$u_{s\ell} = V_0\left[1 - \exp\left(-\frac{h_m}{R_g T_m}\frac{T_{l,I} - T_m}{T_{l,I}}\right)\right] \tag{14}$$

where V_0 is the maximum interface velocity, R_g is the gas constant for the metal, and $T_{l,I}$ is the interfacial temperature. The interfacial temperature, $T_{l,I}$, is higher than melting point, T_m, during melting and lower than melting point during solidification.

For the liquid-vapor interface, energy balance at the interface and evaporation rules derived from kinetics laws will be applied to find its temperature, velocity, hence location [36]. The energy balance at the liquid-vapor interface is:

$$\rho h_{\ell v} u_{\ell v} + \sigma\varepsilon(T_{\ell v}^4 - T_\infty^4) = -k_l\frac{\partial T_l}{\partial x} \tag{15}$$

where $h_{\ell v}$ is the latent heat of evaporation of gold, $u_{\ell v}$ is the velocity of the interface, $T_{\ell v}$ is the temperature of the interface. With known interface velocity, eq. (15) will be used to calculate the interface temperature $T_{\ell v}$.

As stated above, to simulate the non-equilibrium evaporation process, wave hypothesis is employed. The velocity of the dynamic evaporation process will be a characteristic speed of sound in the two-phase region of the fluid. The chosen speed will be that of the coexistence side of the liquidus line which is the low volume boundary of the two-phase region. Because of lacking of experimental data, this

value will be calculated based on equation of state. The sound speed is given by: [37, 38]

$$c = \frac{dp}{dT}\left(\frac{T}{\rho^2 C_V}\right)^{\frac{1}{2}} \tag{16}$$

To calculate this speed, Van der Wal's equation will be employed. The evaporation sound speed is evaluated according to eq. (16) on the liquidus line of the two-phase area.

NUMERICAL METHOD AND INTERFACE TRACKING

In each time step, an iterative procedure will be employed to deal with the non-linear relationship between electron energy equation, lattice energy equation, solid-liquid interface and liquid-vapor interface. Discretized electron energy equation (1) will be solved first using TDMA (TriDiagonal Matrix Algorithm), then the lattice energy equation (2). For the first iteration step in a time step, coefficients in these equations are evaluated based on the temperature of last time step. After obtaining an estimated electron and lattice temperature field, the velocity and temperature of solid-liquid interface will be calculated by using the method provided in Ref. [39], the velocity and temperature of solid-liquid interface will be calculated by using the method provided in Ref. [36].

RESULTS AND DISCUSSION

The irradiation of the laser pulse on a gold particle will be simulated based on the method described above. The thermophysical and optical properties are given in Table 1.

First of all, to justify the current model, the energy balance is checked. For each point on the particle surface, the local incident energy density J is:

$$J = \int_0^{2\pi}\int_0^\pi J_0\sin\varphi\, d\varphi d\omega = 4\pi J_0 \tag{17}$$

J will also be referred to as laser fluence directly hereafter in this paper because it equals to the totally deposited energy divided by surface area. Define E as the total energy deposited on the surface of a single particle:

$$E = (1 - R)4\pi r_0^2 J \tag{18}$$

On the other hand, in the numerical simulation, if S is defined as the energy absorbed by the particle, it is related to S_0 in eq. (1) as an integration over the volume of the particle and time:

$$S = \int_{-\infty}^{+\infty}\int S_0\, dvdt \tag{19}$$

When the particle size is large enough, E and S should be equal to guarantee energy balance in the computation. We calculated E and S with different particle size and different values of $(\delta + \delta_b)$ and found that S/E is a simple function of $r_0/(\delta + \delta_b)$. The dependence of S/E on $r_0/(\delta + \delta_b)$ is plotted in Fig. 3. It can be seen that with small particle size, because of the penetration, part of the incident laser will escape from the other side of the particle, which causes a small ratio of E/S. However, when the particle size is relatively large, for example, when $r_0/(\delta + \delta_b) > 4$, the energy absorbed by the particle S

Copyright © 2011 by ASME

Table 1 Thermophysical properties of gold

Property		Value
Coefficient for electronic heat capacity, B_e		70[28]
Material constant, A_e		1.2×10^7[32]
Material constant, B_1		1.23×10^{11}[32]
Electron-lattice coupling factor at room temperature, G_{RT} (W/m^3 K)	Solid	2.2×10^{16}[32]
	Liquid	2.6×10^{16}[32]
Specific heat, C_p (J/kg K)	Solid	$105.1 + 0.2941 T_1 - 8.731 \times 10^{-4} T_1^2$ $+ 1.187 \times 10^{-6} T_1^3 - 7.051 \times 10^{-10} T_1^4$ $+ 1.538 \times 10^{-13} T_1^5$[15]
	Liquid	163.205[33]
Latent heat of evaporation at T_b, h_{lv} (J/kg)		1.698×10^6[40]
Latent heat of fusion, h_m (J/kg)		6.373×10^4[40]
Molar weight, M (kg/kmol)		196.967[40]
Reflection coefficient, R		0.6
Universal gas constant, R_u (J/K kmol)		8314.0
Boiling temperature, T_b (K)		3127
Critical temperature, T_c (K)		5590
Melting temperature, T_m (K)		1336
Fermi temperature, T_F (K)		6.42×10^4
Limit velocity, V_0 (m/s)		1300[33]
Coefficient for electronic conductivity, χ (W/m K)		353[30]
Optical penetration depth, δ (nm)		20.6
Ballistic range, δ_b (nm)		105[33]
Thermal conductivity at equilibrium, k_{eq} (W/m K)	Solid	$320.973 - 0.0111 T_1 - 2.747 \times 10^{-5} T_1^2$ $-4.048 \times 10^{-9} T_1^3$
	Liquid	$37.72 + 0.0711 T_1 - 1.721 \times 10^{-5} T_1^2$ $+1.064 \times 10^{-9} T_1^3$
Density, ρ (kg/m^3)	Solid	19.3×10^3
	Liquid	17.28×10^3

still not equals to the energy deposited on the surface E. This is because in the current model, not all laser beams are perpendicular to the surface, for those laser beams that have a small angle of φ, it is very easy to penetrate the surface layer and escape the particle. To prove this, an angle restriction is implemented to the laser beam, only the beams with an incidental angle φ (Fig. 2) between $\frac{\pi}{2} \pm \frac{\pi}{20}$ will be considered in the calculation of S_0 in eq.(9). Under this condition, the S/E ratio is lifted a lot and reaches 1 when the particle size is large enough.

The computation results obtained from the current model is then compared with the old model we used in our previous work [24]. The particle size is relatively large, with diameter equals to 1.0 µm. Figure 4 shows the comparison of solid-liquid interfacial temperature and position. It can be seen that the difference between maximum temperatures is less than 1.5%. This proves that when the particle size is large, the difference between the two models is small, which is in accordance with Fig. 3.
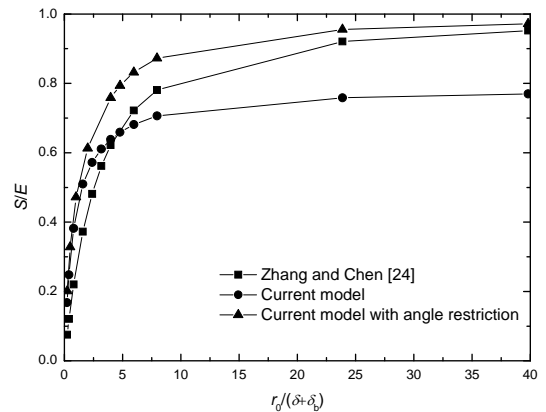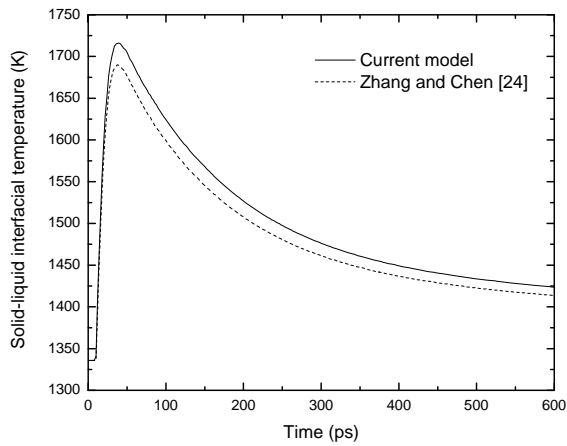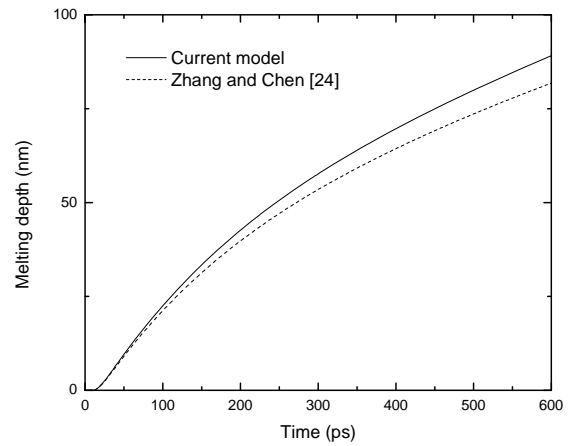

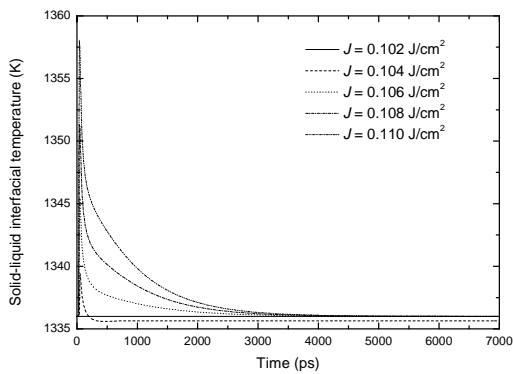Fig. 3 Energy balance with different particle size

(a) Solid-liquid interfacial temperature
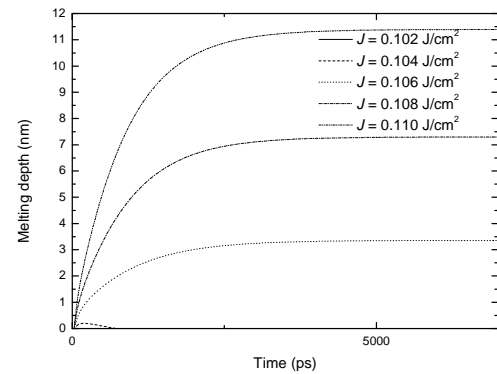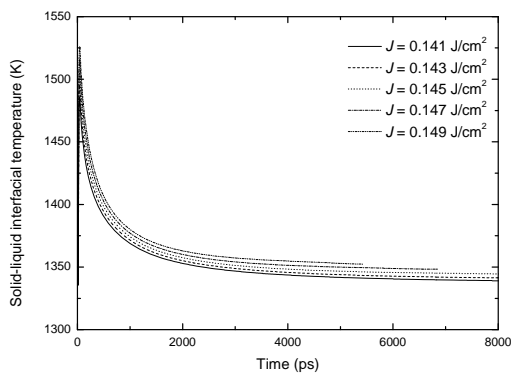

(b) Melting depth

Fig. 4 Comparison between different models

(a) Melting interface temperature (J = 0.102~0.110 J/cm^2)

(b) Melting depth (J = 0.102~0.110 J/cm^2)

(c) Melting interface temperature (J = 0.141~0.149 J/cm^2)
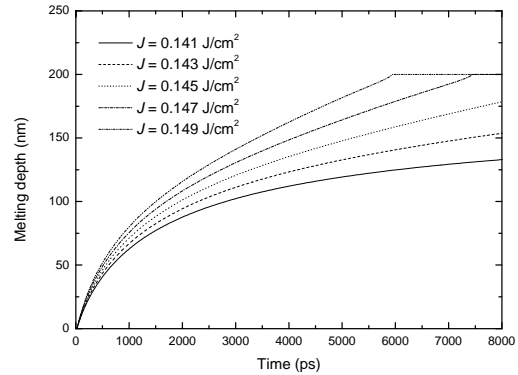
(d) Melting depth (J = 0.141~0.149 J/cm^2)

Fig. 5 Melting process when r_0 = 200 nm

With different laser fluence, the irradiation process is calculate for the case that the laser duration equals to 100 fs and particle diameter equals to 400 nm, the results are shown in Fig. 5. When the laser energy increases gradually, the phase change process shows different characteristics. When effective laser fluence J equals to 0.102 J/cm^2, no melting takes place. When the fluence increases to 0.104 J/cm^2, a thin sub-surface layer melts then resolidifies, as shown in Fig. 5(b), and the final surface temperature decreases to a value below the melting point. When the fluence equals to 0.106 J/cm^2, resolidification no longer occurs. The solid-liquid interface moves to a certain depth then stops. This is because the current model depicts a single particle. The only way to cool down the heated metal is radiation on the surface, which takes much longer time to reach resolidification than the time span covered by the calculations we conducted. When the fluence is between the ranges of 0.106 J/cm^2 to 0.145 J/cm^2, there is always a solid part at the center of the particle. When the temperature in the particle reaches equilibrium, it always equals to the melting point 1336K. When fluence is above 0.145 J/cm^2, the particle is completed melted, and the final temperature will be higher than melting point.
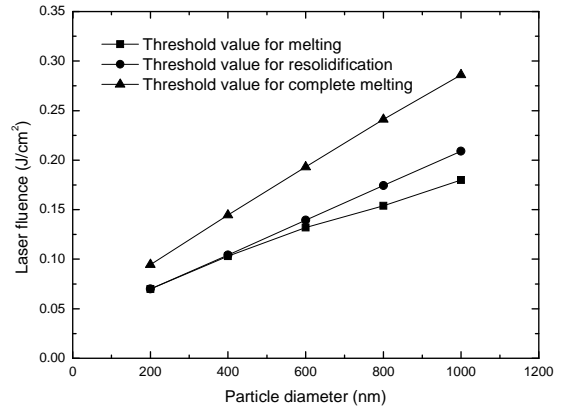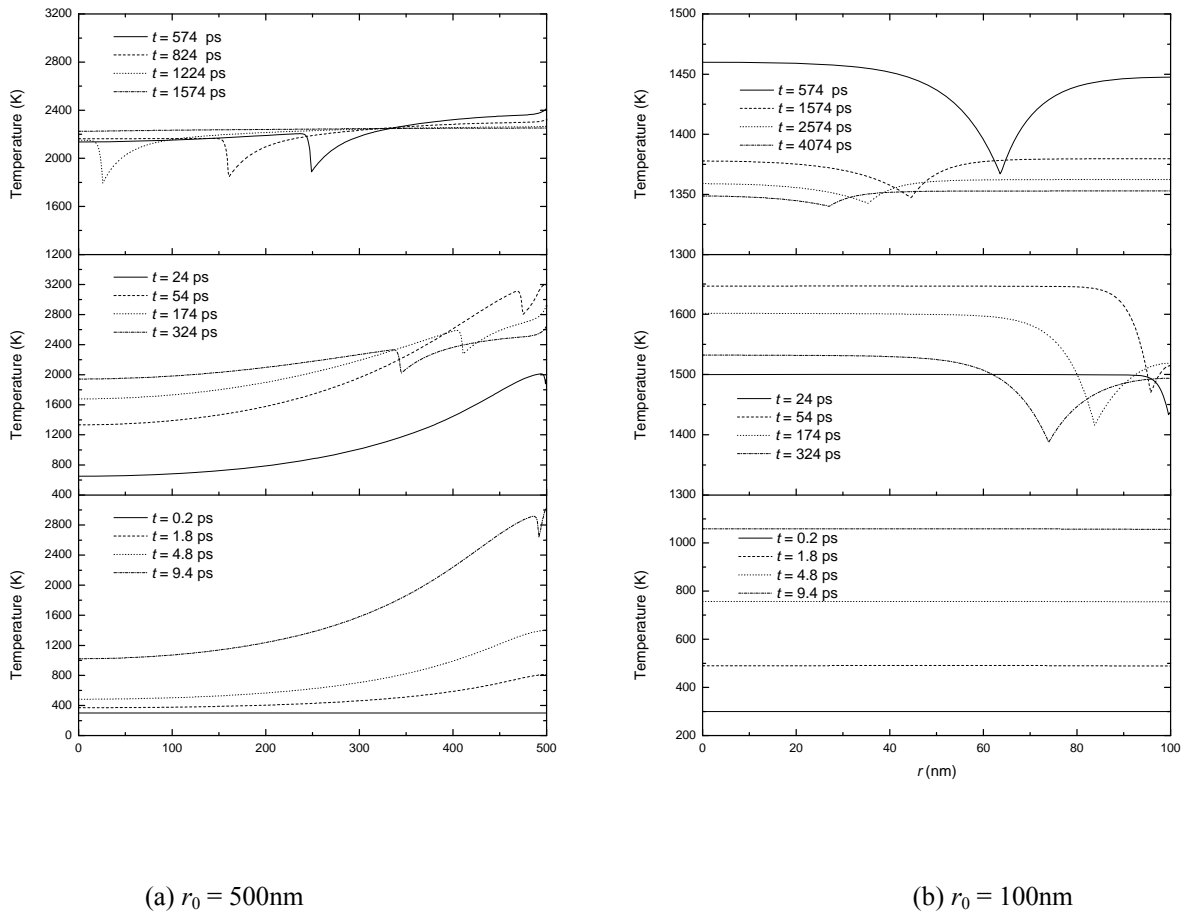

Fig. 6 Threshold values of laser fluence

(a) $r_0 = 500$nm

(b) $r_0 = 100$nm

Fig. 7 Comparison of temperature profile for different particle sizes

Based on the above discussion, we can define three threshold value for J. The first is the threshold value for melting, J_1, below which no melting takes place. The second is the threshold value for resolidification, J_2, above which no resolidification takes place. The third is the threshold value for complete melting, J_3, above which the particle will be melted completely. For different sizes of particles, these values are plotted in Fig. 6. It can be seen that these values are related to particle size almost linearly and larger particles have higher threshold values. When the particle size decreases, the window between melting and complete melting threshold values is smaller, which means for laser sintering with small particles, it is more difficult to find an appropriate fluence value if partial melting is wanted.

Another interesting phenomenon we noticed for small particle in the simulation is the temperature profile. Figure 7(a) shows the temperature distribution along the r-direction at different times when particle diameter equals to 1000 nm, which is relatively large. They are very similar to the results of our previous works [26, 36]. However, when the particle size decreases to 100 nm, as shown in Fig. 7(b), the temperature at the center of the particle rises almost at the same time with surface temperature. At the time of 24 ps, the surface temperature decreased significantly when melting starts because the latent heat for melting consumes a lot of energy at the interface. The latent heat also causes a dip in the temperature profile at the place of the solid-liquid interface when the solid-fluid interface proceeds to the center of the particle.
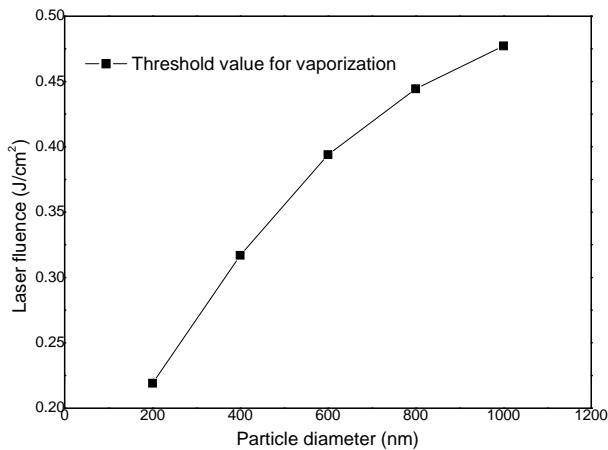

Fig. 8 Threshold value of laser fluence for vaporization

When the laser fluence is high enough, vaporization takes place. We also performed calculation to identify the threshold value of J for vaporization. Figure 8 shows this value with different particle size. Compared with Fig. 6, this value is much higher under same particle size. This means that to achieve sintering, even if complete melting is needed, the laser fluence needed will not cause vaporization.

Small sized particle also shows different characteristic at high laser fluence. Figure 9 shows the time relationship between melting and vaporization with different particle size. When the particle is large, diameter equals to 1000 nm, vaporization takes place at very early stage of melting and it lasts only a very short period of time in comparison with melting. But for small particle with diameter of 200 nm, the whole particle melted completely very fast, and the high temperature caused a relatively long time of vaporization, as shown in Fig. 9(b).
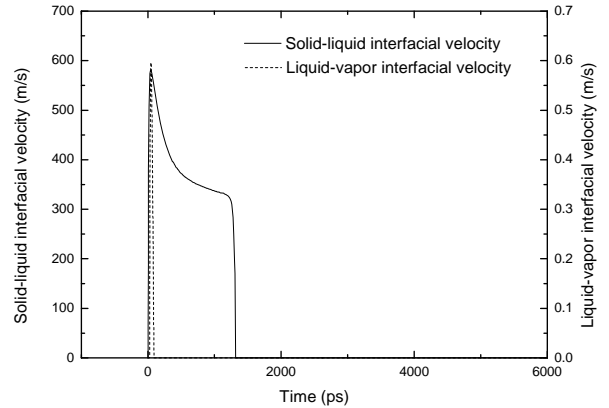
(a) $r_0 = 500$nm, $J = 0.5$ J/cm^2
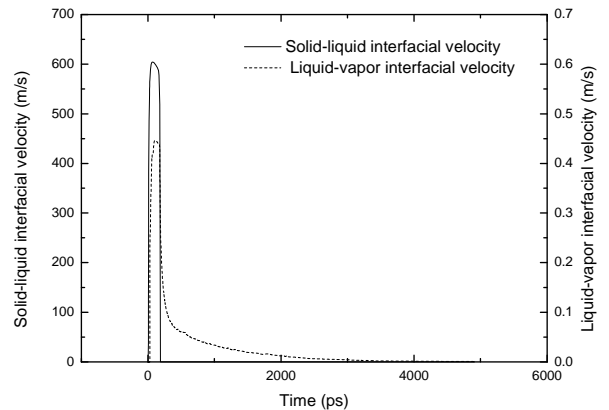
(b) $r_0 = 100$nm, $J = 0.24$ J/cm^2

Fig. 9 Relationship of melting and vaporization under different particle size

CONCLUSION

The effects of particle size on phase change processes are studied numerically when a nanosized particle is irradiated by femtosecond laser pulse. An improved single particle model is introduced to enable the simulation when particle size is comparable to the optical penetration depth. Based on the calculation with different diameters and laser fluences, the following conclusions are made.

Copyright © 2011 by ASME

1. When the laser energy increases, phase changes show different characteristics in the particle. When the fluence is higher than a certain value, such as 0.103 J/cm^2 for diameter of 400 nm, no resolidification takes place for the time range studied. When the fluence is higher than this value, a layer of liquid metal remains at the end of the calculation and temperature remains at melting point. When the fluence is high enough, complete melting can be achieved.
2. The threshold values of laser fluence to reach different melting stages are compared for different particle sizes and it is found that for smaller particles, the difference between melting threshold value and complete melting threshold value is also smaller. This means for small particles, it is more difficult to find appropriate laser fluence to achieve partial melting.
3. To achieve vaporization, the laser fluence must be much higher than the complete melting threshold value. This means no vaporization would happen if partial melting is wanted.
4. For small particles, complete melting can be finished in a very short period of time, while evaporation will last much longer.

ACKNOWLEDGEMENT

REFERENCES

[1] Deckard, C.R., 1988, "Selective Laser Sintering," Ph.D. thesis, University of Texas, Austin, TX.
[2] Deckard, C.R., 1989, Method and apparatus for producing parts by selective sintering, US Patent No. 4, 538.
[3] Deckard, C.R., and Beaman, J.J., 1987, "Solid freeform fabrication and selective powder sintering", Proc. 15th NAMRC-SME, Bethlehem, PA, pp. 636–640.
[4] Kumar, S., 2010, "Selective laser sintering: Recent advances", 4th Pacific International Conference on Applications of Lasers and Optics, Wuhan, China, pp. 8.
[5] Tolochko, N.K., Mozzharov, S.E., Yadroitsev, I.A., Laoui, T., Froyen, L., Titov, V.I., and Ignatiev, M.B., 2004, "Balling processes during selective laser treatment of powders," Rapid Prototyping Journal, 10(2), pp. 78-87.
[6] Bunnell, D.E., 1995, "Fundamentals of Selective Laser Sintering of Metals," Ph.D. thesis, University of Texas: Austin, TX.
[7] Manzur, T., DeMaria, A.J., Chen, W., and Roychoudhuri, C., 1996, "Potential role of high-power laser diode in manufacturing," Proceedings of SPIE, Vol. 2703.
[8] Abe, F., Costa Santos, E., Kitamura, Y., Osakada, K., and Shiomi, M., 2003, "Influence of forming conditions on the titanium model in rapid prototyping with the selective laser melting process," Proceedings of the Institution of Mechanical Engineers, Part C: Journal of Mechanical Engineering Science, 217(1), pp. 119-126.
[9] Su, W.N., Erasenthiran, P., and Dickens, P.M., 2003, "Investigation of fully dense laser sintering of tool steel powder using a pulsed Nd: YAG laser," Proceedings of the Institution of Mechanical Engineers, Part C: Journal of Mechanical Engineering Science, 217(1), pp. 127-138.
[10] Morgan, R., Sutcliffe, C.J., and O'Neill W., 2001, "Experimental investigation of nanosecond pulsed Nd:YAG laser re-melted pre-placed powder beds," Rapid Prototyping Journal, 7(3), pp. 159-172.
[11] Beal, V.E., Erasenthiran, P., Hopkinson, N., Dickens, P., and Ahrens, C.H., 2008, "Scanning strategies and spacing effect on laser fusion of H13 tool steel powder using high power Nd:YAG pulsed laser," International Journal of Production Research, 46(1), pp. 217-232.
[12] Fischer, P., Blatter, A., Romano, V., and Weber, H.P., 2005, "Selective laser sintering of amorphous metal powder," Applied Physics A: Materials Science and Processing, 80(3), pp. 489-492.
[13] Fischer, P., Leber, H., Romano, V., Weber, H.P., Karapatis, N.P., Andre, C., and Glardon, R., 2004, "Microstructure of near-infrared pulsed laser sintered titanium samples," Applied Physics A: Materials Science and Processing, 78(8), pp. 1219-1227.
[14] Fischer, P., Romano, V., Blatter, A., and Weber, H.P., 2005, "Highly precise pulsed selective laser sintering of metallic powders," Laser Physics Letters, 2(1), pp. 48-55.
[15] Fischer, P., Romano, V., Weber, H.P., Karapatis, N.P., Boillat, E., and Glardon, R., 2003, "Sintering of commercially pure titanium powder with a Nd:YAG laser source," Acta Materialia, 51(6), pp. 1651-1662.
[16] Fischer, P., Romano, V., Weber, H.P., and Kolossov, S., 2004, "Pulsed laser sintering of metallic powders," Thin Solid Films, 453-454, pp. 139-144.
[17] Shishkovsky, I.V., Volova, L.T., Kuznetsov, M.V., Morozov, Y.G., and Parkin, I.P., 2008, "Porous biocompatible implants and tissue scaffolds synthesized by selective laser sintering from Ti and NiTi," Journal of Materials Chemistry, 18(12), pp. 1309-1317.
[18] Gusarov, A.V., 2010, "Radiation transfer in metallic-powder beds during laser forming," Quantum Electronics, 40(5), pp. 451-459.
[19] Yilbas, B.S., 1995, "Study into a numerical solution for a pulsed CO_2 laser heating process," Numerical Heat Transfer; Part A: Applications, 28(4), pp. 487-502.
[20] Yilbas, B.S., Sami, M., and Abualhamayel, H.I., 1998, "3-dimensional modeling of laser repetitive pulse heating: A phase change and a moving heat source considerations," Applied Surface Science, 134(1-4), pp. 159-178.
[21] Rostami, A.A., and Raisi, A., 1997, "Temperature distribution and melt pool size in a semi-infinite body due to a moving laser heat source," Numerical Heat Transfer; Part A: Applications, 31(7), pp. 783-796.

[22] Fischer, P., Karapatis, N., Romano, V., Glardon, R., and Weber, H.P., 2002, "A model for the interaction of near-infrared laser pulses with metal powders in selective laser sintering," Applied Physics A: Materials Science and Processing, 74(4), pp. 467-474.

[23] Petrushina, M.V., Pogudo, E.L., and Chivel, Y.A., 2006, "Simulation of the process of sintering of spherical powders under the effect of pulsed laser radiation," High Temperature, 44(1), pp. 151-155.

[24] Zhang, Y., and Chen, J.K., 2008, "Ultrafast melting and resolidification of gold particle irradiated by pico- to femtosecond lasers," Journal of Applied Physics, 104(5), pp. 05491001-05491009.

[25] Shi, Y., Zhang, Y., and Konrad, C., 2007, "Solid-liquid-vapor phase change of a subcooled metal powder particle subjected to nanosecond laser heating," Nanoscale and Microscale Thermophysical Engineering, 11(3-4), pp. 301-318.

[26] Konrad, C., Zhang, Y., and Shi, Y., 2007, "Melting and resolidification of a subcooled metal powder particle subjected to nanosecond laser heating," International Journal of Heat and Mass Transfer, 50(11-12), pp. 2236-2245.

[27] Anisimov, S.I., Kapeliovich, B.L., and Perel'man, T.L., 1974, "Electron emission from metal surfaces exposed to ultra-short laser pulses," Sov. Phys. JETP, 39(2), pp. 375-377.

[28] Qiu, T.Q., and Tien, C.L., 1993, "Heat transfer mechanisms during Short-Pulse laser heating of metals," ASME J. Heat Transfer, 115(4), pp. 835-841.

[29] Chen, J.K., Tzou, D.Y., and Beraun, J.E., 2006, "A semiclassical two-temperature model for ultrafast laser heating," International Journal of Heat and Mass Transfer, 49(1-2), pp. 307-316.

[30] Anisimov, S.I., and Rethfeld, B., 1997, "Theory of ultrashort laser pulse interaction with a metal," Proceedings of SPIE - The International Society for Optical Engineering.

[31] Klemens, P.G., and Williams, R.K., 1986, "Thermal conductivity of metals and alloys," International Metals Reviews, 31(5), pp. 197-215.

[32] Chen, J.K., Latham, W.P., and Beraun, J.E., 2005, "The role of electron-phonon coupling in ultrafast laser heating," Journal of Laser Applications, 17(1), pp. 63-68.

[33] Kuo, L.-S. and Qiu, T., 1996, "Microscale energy transfer during picosecond laser melting of metal films, " ASME Heat Transfer Division Publication HTD, 323(1), pp. 149-157.

[34] Wellershoff, S.S., Hohlfeld, J., Güdde, J., and Matthias, E., 1999, "The role of electron-phonon coupling in femtosecond laser damage of metals," Applied Physics A: Materials Science and Processing, 69(7), pp. S99-S107.

[35] Faghri, A., and Zhang, Y., 2006, *Transport Phenomena in Multiphase Systems*, Elsevier Academic Press, Burlington, MA.

[36] Huang, J., Zhang, Y. and Chen, J.K., 2011, "Superheating in Liquid and Solid Phases during Femtosecond Laser Pulse Interaction with Thin Metal Film," Applied Physics A: Materials Science and Processing. (in press)

[37] Bennett, F.D., 1965, "Vaporization waves as a general property of high temperature matter, " Physics of Fluids, 8(8), pp. 1425-1427.

[38] Bennett, F.D., 1971, "Vaporization-Wave Transitions", *Physics of High Energy Density*, P. Caldirola and H. Knoepfel, eds., Academic Press, New York, NY.

[39] Zhang, Y., and Chen, J.K., 2008, "An interfacial tracking method for ultrashort pulse laser melting and resolidification of a thin metal film," Journal of Heat Transfer, 130(6), pp. 06240101-06240110.

[40] Barin, I., 1993, *Thermochemical data of pure substance, Part I*, Wiley VCH, New York, NY.